IAC-14-C1.4.2

A DIRECT ADAPTIVE CONTROL LAW USING MODIFIED RODRIGUES PARAMETERS FOR ISS ATTITUDE REGULATION DURING FREE-FLYER CAPTURE OPERATIONS

Jian-Feng Shi
MDA Corporation, Canada, Jian-Feng.Shi@mdacorporation.com

Steve Ulrich
Carleton University, Canada, Steve.Ulrich@carleton.ca

A direct adaptive control law is developed for a robust International Space Station attitude regulation during robotic capture of a free-flyer by the Space Station Remote Manipulator System. The proposed output feedback direct adaptive controller is developed from the Simple Adaptive Control theory, and makes use of the Modified Rodrigues Parameters. The performance of the adaptive controller is examined in MacDonald, Dettwiler and Associates Space Station Portable Operations Training Simulator; a high-fidelity multibody flexible dynamic simulation facility. SPOTS simulation results are provided for an ISS free-flyer capture of a SpaceX Dragon-like space vehicle with the flexible SSRMS manipulator. Simulation results highlight the improved performance and robustness to parametric and dynamics modeling uncertainties of the proposed novel attitude control approach when compared with an attitude Proportional-Derivative controller.

I. INTRODUCTION

Spacecraft rendezvous and docking is an important element of on-orbit servicing (OOS). Using a robotic arm to capture a target spacecraft for the purpose of docking add operation flexibility in the mission planning and allows lighter and simpler docking interfaces. The method of free-flyer capture (FFC) was initially tested and perfected during Space Shuttle operations in which varieties of free-flying satellite bodies were captured by the Space-shuttle Remote Manipulator System (SRMS). Theses satellite bodies include the Spartan satellite, the Wake Shield Facility (WSF), and the Hubble Space Telescope (HST). Over the years, various FFC and docking missions ranging from small satellites such as the Japan Aerospace Exploration Agency (JAXA) Engineering Test Satellite #7 (ETS-7)[1] and Defense Advanced Research Projects Agency (DARPA) Orbital Express (OE),[2] to large space platform such as the HST Servicing Mission[3] and the International Space Station (ISS) cargo spacecraft.[4] A recent survey by Flores-Abad *et al.*[5] provides a comprehensive list of free-flyer spacecraft robotic operations and ground test facilities. The FFC operations are traditionally performed by human crew operator tracking and capturing the free-flyer from the manipulator End-Effector (EE) camera. Later, robotic satellite operations such as those on the OE mission employed fiduciary markers on the target spacecraft to aid autonomous tracking and capture of the target satellite.[2] In the case of the ISS capture of a free-flyer vehicle, the Space Station Remote Manipulator System (SSRMS) manoeuvres into a free-flyer Inner Capture Box (ICB) zone where the free-flyer cargo vehicle is holding roughly 10 meters nadir to the ISS.[6] Once the robotic operator on the ISS determines the relative vehicle motion is acceptable for robotic capture, the free-flyer is then commanded to a free-drift mode while the SSRMS Latching End Effector (LEE) is manoeuvred towards the Flight Releasable Grapple Fixture (FRGF) or Power and Video Grapple Fixture (PVGF) on the free-flyer cargo vehicle. The SSRMS LEE then captures the vehicle with three snare cables in the LEE cavity. To date, there are three types of the free-flyer cargo vehicles making use of this approach; these are the JAXA H-II Transfer Vehicle (HTV), the Space Exploration Technologies Corporation (SpaceX) Dragon Vehicle, and the Orbital Science Corporation (OSC) Cygnus Vehicle. The ISS logistics cargo vehicles using FFC for docking are shown in Figure 1. The first robotic capture operation on the ISS was the HTV-1 vehicle on GMT-2009/260. By GMT-2014/197, 4 HTV, 4 Dragon, and 3 Cygnus vehicles have visited the ISS while using the SSRMS for capture and release operations.

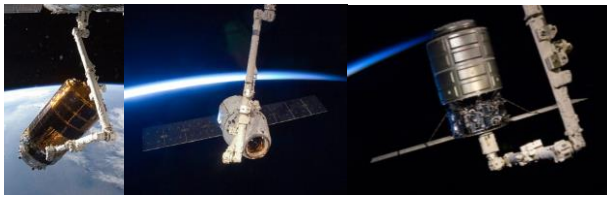

Figure 1 ISS Logistic Cargo Vehicles (HTV left, Dragon centre, Cygnus right). *Photo Credit NASA*.

The ISS FFC operation is limited by the interface misalignment between the LEE and the free-flyer Grapple Fixture (GF) as higher interface misalignment

may generate higher capture loads in the SSRMS and connecting interfaces (SSRMS, LEE, and FRGF shown in Figure 2). The higher capture loading is due to greater torque energy applied into the system so the rigidization motor can correct the free-flyer interface misalignments between the LEE cam pockets and the GF cam arms during the rigidization operation.

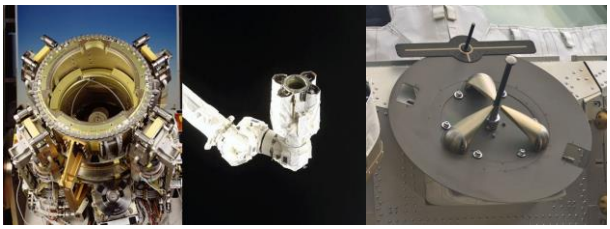

Figure 2 LEE (left, centre), FRGF (right). *Photo Credit MDA, CSA, NASA.*

As consequence of a possible large misalignment capture scenario, the ISS attitude control system may be required to compensate for higher external torques using the ISS Control Moment Gyros (CMG).[7] In this context, the main contribution of this paper is to evaluate a new adaptive control method of control to minimize/remove ISS motion and attitude bias build-up as the result of large interface misalignment FFC.

This paper is organized as follows: Section II defines the control objective, Section III presents the ISS attitude control law and the new adaptive controller developed recently by Shi *et al.*[15], Section IV describes the flexible multi-body simulation facility SPOTS, Section V outlines the flexible modeling of the ISS, and Section VI provides the simulation results demonstrating the performance of the adaptive control system under large dynamic uncertainties. Finally, Section VII summarizes this study.

II. CONTROL OBJECTIVE

Attitude control of a servicer spacecraft during capture manoeuvres has been explored in many past studies; an example of this is the motion-following control algorithm as described by Tsuda and Nakasuka.[8] In cases of the Space Shuttle HST missions, ETS-7, and OE, both the target vehicle and chaser vehicle remained in free-drift during the FFC process.[1,2,5] A free-drifting vehicle will have its Reaction Control System (RCS) disabled. Bedrossian *et al.*[9-12] describe several attitude guidance and control methods for the ISS including the Zero-Propellant Manoeuvre™ (ZPM), contingency attitude control recovery, ISS to Space Shuttle and payload manoeuvring operations.

For a FFC, the attitude control objective is defined as a regulation task, i.e., stabilizing both the attitude and angular velocity back their nominal values. To quantify the control objective, the quaternion and angular rate error, denoted by $\mathbf{q}_{err}$ and $\boldsymbol{\omega}_{err}$ are defined as

$$\mathbf{q}_{err} = \begin{bmatrix} \boldsymbol{\varepsilon}_{err}^{T} & \eta_{err} \end{bmatrix}^{T} = \mathbf{q}_{d} \otimes \mathbf{q} \qquad [1]$$

$$\boldsymbol{\omega}_{err} = \boldsymbol{\omega}_{d} - \boldsymbol{\omega} \qquad [2]$$

where $\mathbf{q}_d$ and $\boldsymbol{\omega}_d$ denote the desired quaternion and angular velocity, respectively given by $\mathbf{q}_d = \mathbf{q}(t_0)$ and $\boldsymbol{\omega}_d = [0;0;0]$ rad/s, and where $\mathbf{q}$ and $\boldsymbol{\omega}$ denote the actual quaternion and angular velocity, respectively.

III. CONTROL LAWS

Proportional-Derivative Control

Bedrossian[9] describe the Proportional-Derivative (PD) control torque $\boldsymbol{\tau}_{PD}$ as

$$\boldsymbol{\tau}_{PD} = \mathbf{J}_{ISS}\left(\mathbf{K}_{p}\boldsymbol{\varepsilon}_{err} + \mathbf{K}_{d}\boldsymbol{\omega}_{err}\right) \qquad [3]$$

where $\mathbf{J}_{ISS}$ denotes the ISS inertia matrix, $\mathbf{K}_p$ is the proportional gain matrix, $\mathbf{K}_d$ is the derivative gain matrix. During ISS capture of the free-flyer logistic cargo vehicles, the free-flyer vehicle manoeuvres into the ICB and is commanded to free-drift while the SSRMS manoeuvres in for capture, the Space Station Program (SSP) flight rule requires the ISS Service Module (SM) Motion Control System (MCS) to be placed in Attitude Hold (AH) using a PD controller[13] where CMG desaturation requests are inhibited.

Simple Adaptive Control

Between the extremes of knowing the motion of the target and having complete free-drift during capture, a direct adaptive control law is developed for a robust spacecraft attitude regulation during robotic FFC of another body in space. The proposed output feedback direct adaptive controller is developed from the Simple Adaptive Control (SAC) theory,[14] and makes use of the Modified Rodriguez Parameters (MRP) to formulate the Euler-Lagrange system into a non-linear square state-space model. The adaptive control gain matrix contains a stabilization component that is adapting to the output tracking error, as well as two ideal model-based feed-forward components to improve the tracking performance. All adaptive control gains are obtained from an integral and proportional term. For completeness, the adaptive attitude control law formulation presented in detail by Shi *et al.*[15] is summarized in this section.

Consider the following attitude control law

$$\boldsymbol{\tau}_{SAC} = \mathbf{T}^T(\boldsymbol{\sigma})\mathbf{u} \quad [4]$$

where $\boldsymbol{\tau}_{SAC}$ is the control torque applied on the ISS, $\mathbf{T}$ is the transformation with the control input $\mathbf{u}$ corresponding to SAC algorithm*

$$\mathbf{u} = \mathbf{K}_e(t)\mathbf{e}_y + \mathbf{K}_x(t)\mathbf{x}_m + \mathbf{K}_u(t)\mathbf{u}_m \quad [5]$$

In Equation [5], $\mathbf{K}_e(t)$ is a stabilizing gain, and $\mathbf{K}_x(t)$ and $\mathbf{K}_u(t)$ are feed-forward gains that contribute to bring the tracking error to zero, $\mathbf{e}_y$ is the output feedback error, $\mathbf{x}_m$ is the ideal model state trajectory to be tracked by the controller, and $\mathbf{u}_m$ is the input of the ideal model, i.e., the desired MRP states. The tracking output error between the output of the ideal model and the actual system, $\mathbf{e}_y$, is used to generate the integral adaptive control gains

$$\dot{\mathbf{K}}_{Ie}(t) = \mathbf{e}_y\mathbf{e}_y^T\boldsymbol{\Gamma}_{Ie} \quad [6]$$

$$\dot{\mathbf{K}}_{Ix}(t) = \mathbf{e}_y\mathbf{x}_m^T\boldsymbol{\Gamma}_{Ix} \quad [7]$$

$$\dot{\mathbf{K}}_{Iu}(t) = \mathbf{e}_y\mathbf{u}_m^T\boldsymbol{\Gamma}_{Iu} \quad [8]$$

where $\boldsymbol{\Gamma}_{Ie}$, $\boldsymbol{\Gamma}_{Ix}$, and $\boldsymbol{\Gamma}_{Iu}$ are matrices of coefficients that determine the rate of SAC algorithm adaptation. Equation [6]-[8] can be written concisely by defining

$$\dot{\mathbf{K}}_I(t) = \begin{bmatrix}\dot{\mathbf{K}}_{Ie}(t) & \dot{\mathbf{K}}_{Ix}(t) & \dot{\mathbf{K}}_{Iu}(t)\end{bmatrix} \quad [9]$$

$$\mathbf{r} = \begin{bmatrix}\mathbf{e}_y^T & \mathbf{x}_m^T & \mathbf{u}_m^T\end{bmatrix}^T \quad [10]$$

such that

$$\dot{\mathbf{K}}_I(t) = \mathbf{e}_y\mathbf{r}^T\boldsymbol{\Gamma}_I \quad [11]$$

where $\boldsymbol{\Gamma}_I$ is the resulting adaptation matrix associated with the integral gain $\mathbf{K}_I(t)$. Although only the integral adaptive gain $\mathbf{K}_I(t)$ is absolutely necessary to guarantee the convergence of the adaptive control system, it is customary to include the adaptive gain $\mathbf{K}_P(t)$ as well, to increase the rate of convergence of the adaptive system toward perfect tracking. Therefore, the adaptive control gains used in Equation [5] are obtained as

$$\mathbf{K}_e(t) = \mathbf{K}_{Pe}(t) + \mathbf{K}_{Ie}(t) \quad [12]$$

$$\mathbf{K}_x(t) = \mathbf{K}_{Px}(t) + \mathbf{K}_{Ix}(t) \quad [13]$$

$$\mathbf{K}_u(t) = \mathbf{K}_{Pu}(t) + \mathbf{K}_{Iu}(t) \quad [14]$$

where the proportional adaptive control terms are defined similarly to the integral terms, as follows

$$\mathbf{K}_{Pe}(t) = \mathbf{e}_y\mathbf{e}_y^T\boldsymbol{\Gamma}_{Pe} \quad [15]$$

$$\mathbf{K}_{Px}(t) = \mathbf{e}_y\mathbf{x}_m^T\boldsymbol{\Gamma}_{Px} \quad [16]$$

$$\mathbf{K}_{Pu}(t) = \mathbf{e}_y\mathbf{u}_m^T\boldsymbol{\Gamma}_{Pu} \quad [17]$$

Defining the proportional gain matrix as

$$\mathbf{K}_P(t) = \begin{bmatrix}\mathbf{K}_{Pe}(t) & \mathbf{K}_{Px}(t) & \mathbf{K}_{Pu}(t)\end{bmatrix} \quad [18]$$

$$\mathbf{K}_P(t) = \mathbf{e}_y\mathbf{r}^T\boldsymbol{\Gamma}_P \quad [19]$$

where $\boldsymbol{\Gamma}_P$ is the resulting adaptation matrix associated with the proportional gain $\mathbf{K}_P(t)$, the total adaptive gain, denoted by $\mathbf{K}(t)$, can be obtained as

$$\mathbf{K}(t) = \mathbf{K}_P(t) + \mathbf{K}_I(t) \quad [20]$$

Making use of Equation [20], the attitude control law (1) can be rewritten concisely as

$$\boldsymbol{\tau} = \mathbf{T}^T(\boldsymbol{\sigma})\mathbf{K}(t)\mathbf{r} \quad [21]$$

MRP Conversion

Due to model or sensor interface restrictions, it is necessary to perform conversions between the rotation matrix and MRP. Similar to Rodrigues Parameters as described by Hughes,[16] the MRP conversion from rotation matrix to and from MRP are as follows:

Let a rotation matrix be

$$\mathbf{C} = \begin{bmatrix} c_{11} & c_{12} & c_{13} \\ c_{21} & c_{22} & c_{23} \\ c_{31} & c_{32} & c_{33} \end{bmatrix} \quad [22]$$

Let

$$\boldsymbol{\Delta} = \begin{bmatrix} c_{23} - c_{32} \\ c_{31} - c_{13} \\ c_{12} - c_{21} \end{bmatrix} \quad [23]$$

If β be one plus the trace of $\mathbf{C}$

* *Kaufman, H., Barkana, I., and Sobel, K., Direct Adaptive Control Algorithms: Theory and Applications, Communications and Control Engineering Series, Springler, New York, NY, 2nd ed., 1997.*

$$\beta = 1 + trace(C) = 1 + c_{11} + c_{22} + c_{33} \quad [24]$$

If $\beta \neq 0$, then

$$\boldsymbol{\sigma} = \frac{\boldsymbol{\Delta}}{\beta \pm 2\sqrt{\beta}} \quad [25]$$

If $\beta = 0$, then

$$\sigma_i = \pm\sqrt{\frac{1 + c_{ii}}{2}}, \quad \forall_i = 1, 2, 3 \quad [26]$$

Equation [27] describes conversion from MRP to rotation matrix

$$\mathbf{C} = \frac{\left(1 - 6\bar{\sigma}^2 + \bar{\sigma}^4\right)\mathbf{1} + 8\boldsymbol{\sigma}\boldsymbol{\sigma}^T + 4\left(\bar{\sigma}^2 - 1\right)\boldsymbol{\sigma}^\times}{\left(\bar{\sigma}^2 + 1\right)^2} \quad [27]$$

IV. SIMULATION FACILITY

The proposed method was experimentally validated on the MacDonald, Dettwiler and Associates (MDA) *Space Station Portable Operations Training Simulator* (SPOTS), a high-fidelity multibody flexible dynamic simulation facility.[17] SPOTS represent the main dynamic simulation tool used by Canadian Space Agency (CSA) for operations and planning of the ISS Mobile Servicing System (MSS). Specifically, the SPOTS software supports MSS flight software verification, flight anomaly resolution, partial operation procedure development/checkout, real-time flight support, ground hardware testing preparation, Common Berthing Mechanism (CBM) interface analysis for NASA End-to-end Berthing Integration Team (EBIT) activities, and NASA dynamic simulator validation. Some examples of past ISS operations analysed by SPOTS include ISS assembly, Extra Vehicular Activity (EVA) operations, robotic Orbit Replacement Unit (ORU) change-outs, manipulator to manipulator payload hand-offs, NASA Robotic Refuelling Mission (RRM) tasks, MSS robotic free-space and contact tasks, and JAXA HTV, SpaceX Dragon, OSC Cygnus free-flyer capture and releases. SPOTS capability includes flexible body dynamics, orbital mechanics, contact dynamics,[18] encapsulated flight software, and integrated robotic models from CSA, JAXA, NASA, and Roscosmos. Outside the SSP CSA Logistics and Sustaining Engineering (L&SE) program, SPOTS was used in the retired Space Shuttle program (in aid of the SRMS ASAD dynamic simulator), HST robotic servicing mission design,[19] Orbital Express mission analysis, Space Infrastructure Servicing (SIS) mission design, Next Generation Canadarm (NGC) simulator engine, Mars rover mission study, and CSA ClearSky orbit debris removal study.

SPOTS *Contact Dynamic Toolkit* (CDT) is a self-contained plug-in module to the SPOTS environment that identifies all the contact regions or points and computes corresponding contact forces and moments as the result of relative movements and contact of designated bodies. Multiple validations of the SPOTS have been performed and described in Ma.[18] Recent validation includes hardware collision tests performed at the MDA facility in Brampton.

V. MODEL DESCRIPTION

The SPOTS model is a dynamic system of elastic chains that obeys the following generic mass-stiffness formulation given by

$$M\ddot{q} + Kq = f \quad [28]$$

where M is the system rigid and elastic mass matrix, K is the system stiffness matrix, f is the total force in modal coordinates, q is the modal coordinate parameter. A system damping term can typically be added to emulate system structural damping. The dynamic model consists of 5 major components, these are:

1. Mass and flexibility model of the ISS, SSRMS, and Free-flyer vehicle
2. Flight Control Software of the MSS including the SSRMS and the LEE
3. Manipulator Joint and Motor Models
4. CDT and Snare/Rigidize model of the LEE and GF
5. ISS Attitude Controller

Each of the major components will be discussed in detail in the following subsections. It should be noted the Earth gravitation force and moment model is also available in SPOTS, however was not enabled since the scope of this study is limited to the ISS reaction to large capture forces in the short term while gravitational forces acts over a longer duration of vehicle orbit. As a result, they can be neglected when compared to the short duration snaring and rigidization forces from the capture.

Mass and Flexibility Models

The SSRMS is modeled with combining multiple elastic bodies each synthesized with flexible springs that are computed from NASTRAN Finite Element Models (FEMs). The link bodies are connected together through a series of one Degrees-of-Freedom (DOF) rotational joints. The SSRMS boom structures have the highest number of vibratory modes in comparison with other manipulator links. The Free-flyer mass properties

are simplified for this study demonstration whereas in real operations more precise mass and stiffness matrices are provided by each of the vehicle/payload Original Equipment Manufacturers (OEMs). In the case of the Dragon vehicle, the pre-flight simulation model would include the FRGF door flexibility and the detailed flexible solar panels. In the SAC demonstration simulation, both ISS and the Dragon class vehicle shall be considered as rigid bodies for first order approximation, where the SSRMS joints are the most flexible system component.

Flight Control Software of the SSRMS and LEE

The flight control software of the MSS consists of flight software for the Robotic Work Station (RWS) called Operations Control Software (OCS); it controls the Arm Control Units (ACU) located on the manipulator booms. These ACU provide arm level commands to the Joint Control Software (JCS) and LEE Control Software (LCS) which controls the joint and LEE motors.

Manipulator and Joint and Motor Models

The SSRMS manipulator joints and motors are modeled to provide realism in joint elasticity and resistive friction. The non-linear elastic joint stiffness of the housing and the gear box are represented. The manipulator joint friction is regularly characterized with SSRMS flight data to monitor for joint degradation as well as to maintain an up-to-date calibration of the SPOTS software. A picture of the SSRMS Yaw Joint is provided in Figure 3.

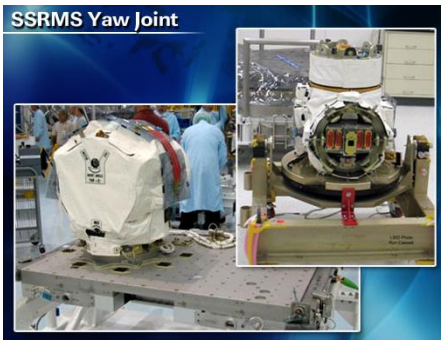

Figure 3 SSRMS Yaw Joint[18] *Photo Credit CSA, NASA*[†]

Contact and Snare/Rigidize Model of the LEE and GF

The interface between the LEE and GF is modeled with snare ring and cables, carriage, and latches. These components are formulated with sets of interacting models representing the snare to GF probe contact, LEE end ring to GF abutment plate and cam arm contact (shown in Figure 4) while providing force feedback to the LEE Motor Modules (LMM). A Force and Moment Sensor (FMS) in the LEE assembly is also modeled in the simulator to monitor loads the same way as the FMS hardware assembly.

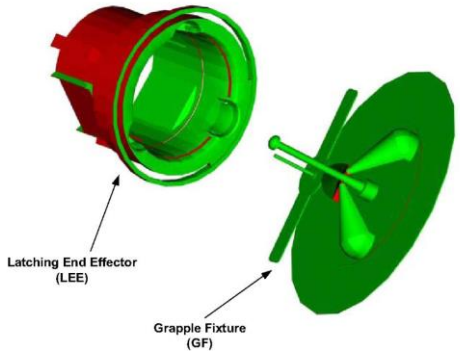

Figure 4 End Effector/Grapple Fixture Contact Model.[19] *Graphic Credit MDA.*

Coordinate Systems

The ISS operates in a circular orbit that is between 350 km to 460 km.[20‡] The ISS vehicle Local Vertical and Local Horizontal (LVLH) is located at the ISS centre-of-mass (COM) with *x* pointing in the direction of orbit motion, *z* pointing nadir towards centre of the Earth, and *y* completing the right hand coordinate system. The free-flyer approach to the ISS shall be measured in the ISS LVLH frame of reference. The Space Station Analysis Coordinate System (ISSACS) is the primary coordinate system for all ISS analysis. It is centred at the integrate truss segment S0. The Space Station Body Coordinate System (ISSBCS) is centred at the ISS COM with the same orientation as ISSACS[21]. The SSRMS End Effector Operator Coordinate System (EEOCS) is a frame that is centred at the LEE tip with *x* pointing outward from the LEE, *z* pointing away from the LEE camera, and *y* making the right hand coordinate system as shown in Figure 5. The GF Position (GFP) Coordinate System is aligned with the EEOCS once the LEE and FRGF is fully rigidized. For all the logistic cargo vehicles, a Structural Coordinate System (SCS) is a mechanical design reference fixed to the spacecraft, where the COM and GFP is located relative to the SCS. A free-flyer Body Coordinate System (BCS) is a coordinate that has the same orientation as the SCS, however is located at the COM of the logistic cargo vehicle.

Mass Properties

For the purposes of this study, similar mass class vehicles for the ISS and Dragon are used as simulation input. Mass properties are provided in Table 1.

[†] *http://www.nasa.gov/images/content/215742main_B03_SSRMS-Yaw-Joint.jpg*

[‡] ISS orbit data can be viewed publicly at *http://www.heavens-bove.com/orbit.aspx?satid=25544*

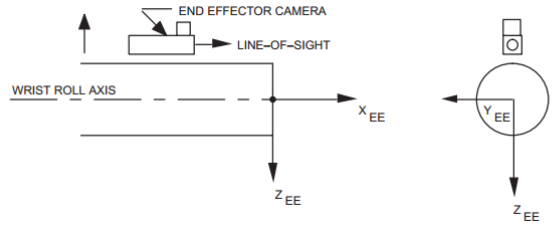

Figure 5 End Effector Operator Coordinate System (EEOCS).[21] *Diagram Credit MDA.*

Description	Value	Units
Dragon Class Vehicle		
Mass[22]	10×10^3	kg
Moment of Inertia $[I_{xx};I_{yy};I_{zz};I_{xy};I_{xz};I_{yz}]$[23]	[20;20;25;0;0;0] $\times10^3$	kg·m^2
ISS Class Vehicle		
Mass[24]	400×10^3	kg
COM from ISSACS	[-5;0;3]	m
Moment of Inertia $[I_{xx};I_{yy};I_{zz};I_{xy};I_{xz};I_{yz}]$[25]	[100;100;200;0;0;0] $\times10^6$	kg·m^2

Table 1 ISS and Dragon Class Vehicle Mass Properties.

ISS Attitude Controller

The ISS attitude controller consists of variety of control methods that are selectable using SPOTS initialization settings. The available options are the SAC and PD controllers with selectable ISS attitude inputs that maybe in the form of Quaternion, MRP and Euler Angles. The ISS attitude control method is described by Bedrossian,[12] the Quaternion PD control law that is proportional to the ISS quaternion ε_1, ε_2, and ε_3 will be used to compare with SAC performance, and the integral term is set to zero, as it is typically done with the actual ISS AH control. The ISS CMG feedback control law is given by

$$\dot{\mathbf{H}}_{cmg} = -\boldsymbol{\tau} - \boldsymbol{\omega}_{ISS}^{\times}\mathbf{H}_{cmg} \qquad [29]$$

where $\boldsymbol{\tau}$ is the control torque applied on the ISS by the CMG, i.e., either $\boldsymbol{\tau}_{PD}$ or $\boldsymbol{\tau}_{SAC}$. $\boldsymbol{\omega}_{ISS}$ denotes the inertial angular velocity of the ISSBCS and $\mathbf{H}_{cmg}$ denotes the total CMG angular momentum which is limited to 14,642 Nms for three operational CMGs.[10] The $\boldsymbol{\omega}_{ISS}^{\times}\mathbf{H}_{cmg}$ term is the gyroscopic torque generated by the total CMG momentum. The torque generated by the CMG $\boldsymbol{\tau}$ is limited to 542 Nm per axis due to CMG saturation.[11] Finally, the equation of motion for the ISS attitude motion can be written as

$$\mathbf{J}\dot{\boldsymbol{\omega}}_{ISS} + \boldsymbol{\omega}_{ISS}^{\times}\mathbf{J}\boldsymbol{\omega}_{ISS} + \dot{\mathbf{H}}_{cmg} + \boldsymbol{\omega}_{ISS}^{\times}\mathbf{H}_{cmg} = \boldsymbol{\tau}_{dist} \qquad [30]$$

where $\boldsymbol{\tau}_{dist}$ denotes the disturbance torque expressed in ISSBCS. The SAC system control diagram is provided in Figure 6.

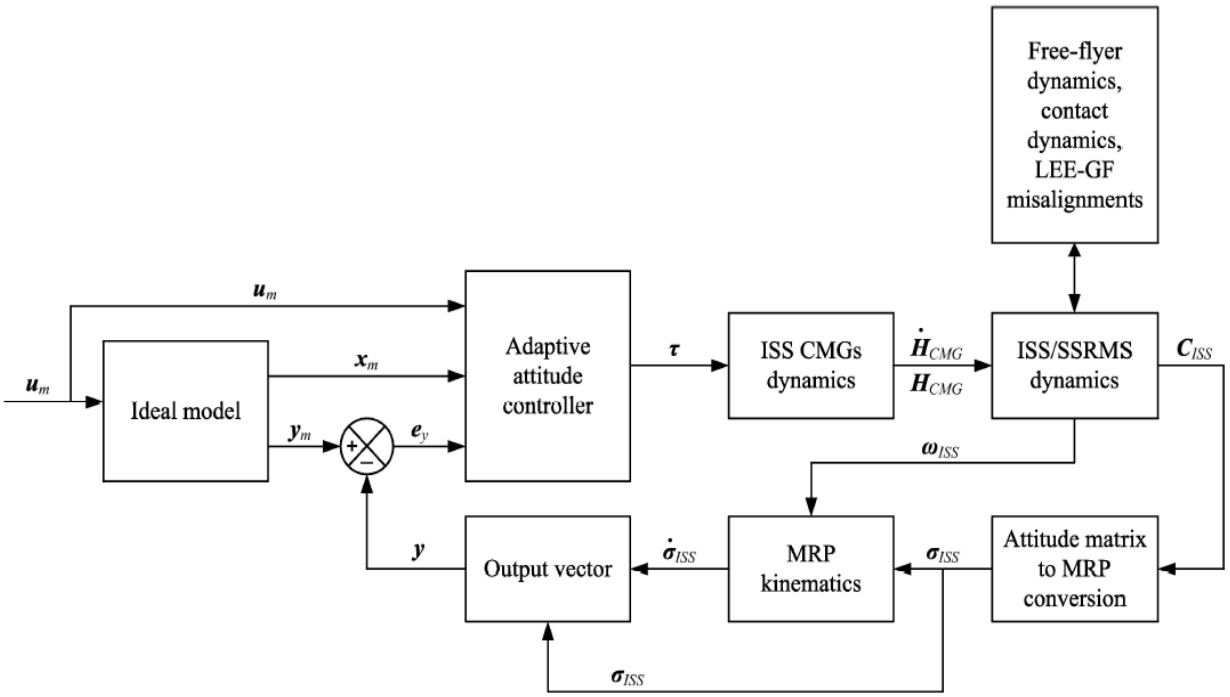

Figure 6 Block Diagram Scheme Illustrating the ISS Implementation of the Adaptive Attitude Controller.[15]

Relative Velocity and EE-GF Misalignments

The EEOCS to GFP capture misalignment and vehicle Initial Condition (IC) pose and rates are provided in Table 2.

Description	Value	Units
EEOCS to GFP Position [*x*; *y*; *z*]	[14; 2; 2]	cm
EEOCS to GFP Orientation[§] [*roll*; *pitch*; *yaw*]	[5; 7; 7]	deg
Free-flyer GFP Linear Velocity Norm relative to ISSACS	33	mm/s
Free-flyer BCS relative to ISS LVLH	0.136	deg/s
ISSBCS Initial Attitude[§] [*roll*; *pitch*; *yaw*]	[1; -3; 0]	deg
ISSBCS Initial Linear/Angular Rate Relative to LVLH	**0**	mm/s; deg/s

Table 2 EEOCS to GFP Misalignment and ISS to Dragon Vehicle Relative Velocity.

VI. SIMULATION RESULTS

FFC Dynamic Characteristics

A load-cell located in the LEE mechanism measures the rigidization force between the LEE and GF interface, this parameter is useful in determining the state of the capture. Figure 7 shows the rigidization force for free-drift, PD and SAC control. It can be shown the capture process completes within the first minute after initiating the capture command. The final rigidization between the LEE and GF reach above 1000 lb_f to secure the free-flyer payload. Once rigidized, the SSRMS returns to a Manual Augmented Mode (MAM) where SSRMS is placed in position hold. It should be noted in a typical flight scenario, the LEE-GF misalignment is nominally much smaller than the worst case values described in Table 2, it is however necessary to simulate larger misalignments to provide maximum flexibility to the astronaut operator.

§ Euler Angles using Pitch-Yaw-Roll Rotation Sequence

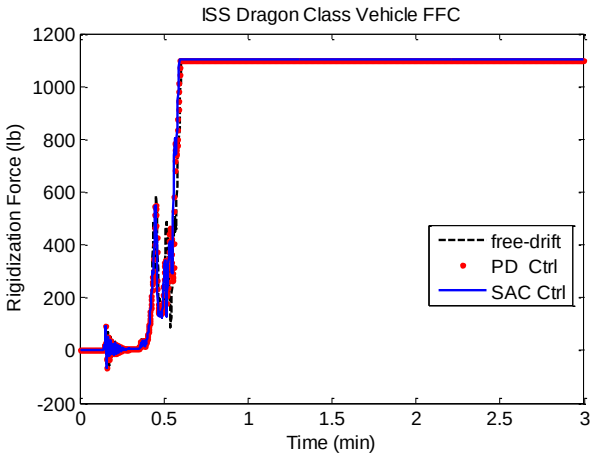

Figure 7 EE Snare Mechanism Rigidization Force.

Controller Gain Tuning

Both PD and SAC control are stable and result in ISS attitude and body rates converging to their target values. The controller gains may be modified to optimize performance. Gain tuning was performed for the PD and SAC controller, selected results of the gain tuning is provided in Figure 8 to Figure 13 for PD and SAC respectively. The gain tuning criteria for PD control is to achieve a balance between signal overshoot and settling time. ISS attitude is mostly affected by the PD derivative gain. Final gain selected for the PD controller are K_p=0.08, K_d=1.0. For the SAC controller, the adaptive gamma parameters are tuned to achieve the optimal control performance. The tuning required balancing signal overshoot with torque controllability. It was observed that as the gamma parameters increase, the CMG torque begins to show noisy oscillations, an example of such undesirable oscillations is show in Figure 14. It can be shown $\boldsymbol{\Gamma}_e$ has the most influence on SAC performance. The final SAC gamma parameters are selected as $\boldsymbol{\Gamma}_e=10^{22}\cdot I_3$, $\boldsymbol{\Gamma}_x=10^{3}\cdot I_6$, $\boldsymbol{\Gamma}_u=10^{7}\cdot I_3$.

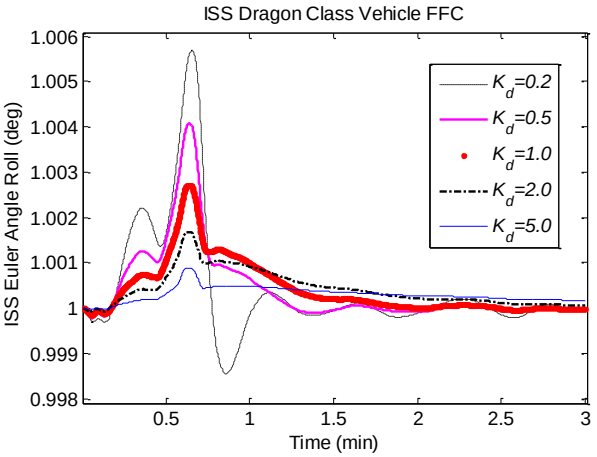

Figure 8 ISS Roll Angle for Various PD K_d Gains.

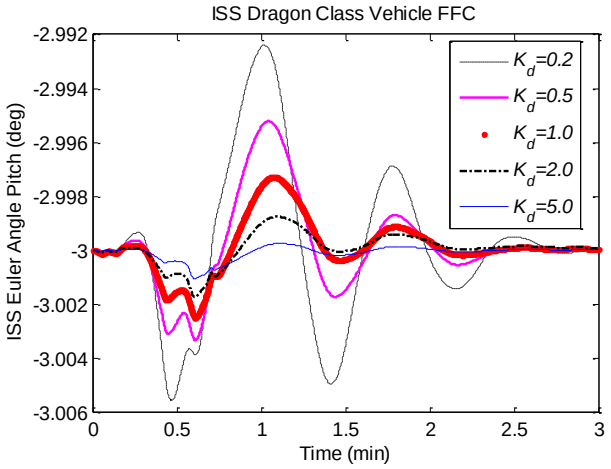

Figure 9 ISS Pitch Angle for Various PD K_d Gains.

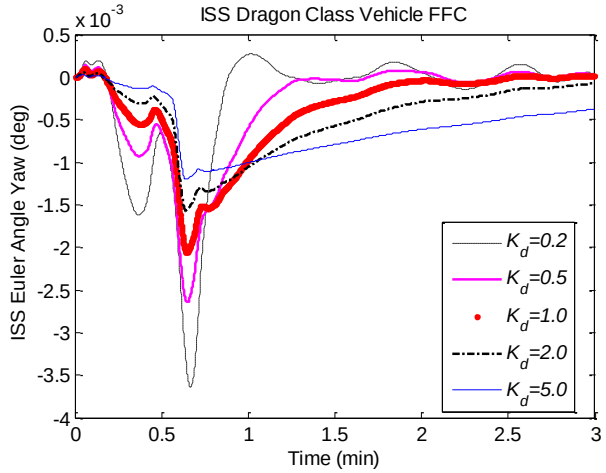

Figure 10 ISS Yaw Angle for Various PD K_d Gains.

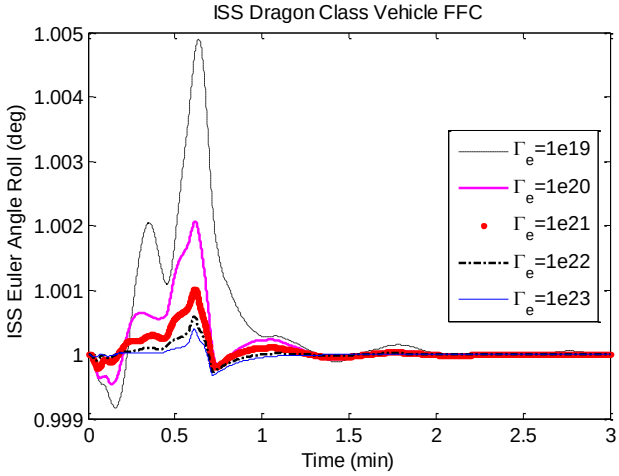

Figure 11 ISS Roll Angle for Various SAC Γ_e Gains.

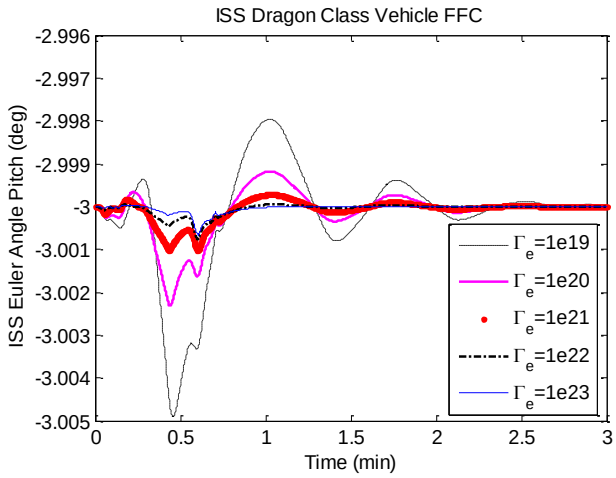

Figure 12 ISS Pitch Angle for Various SAC Γ_e Gains.

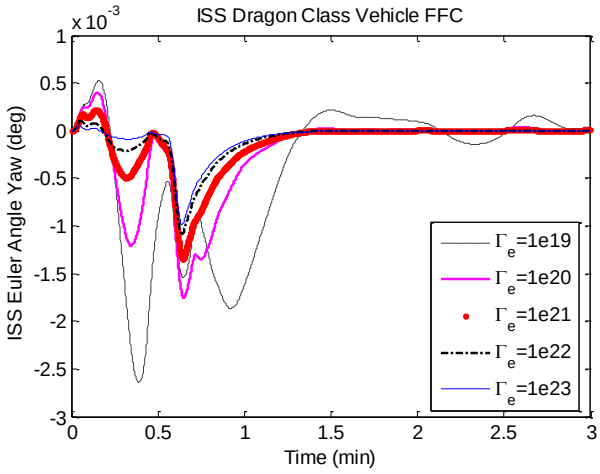

Figure 13 ISS Yaw Angle for Various SAC Γ_e Gains.

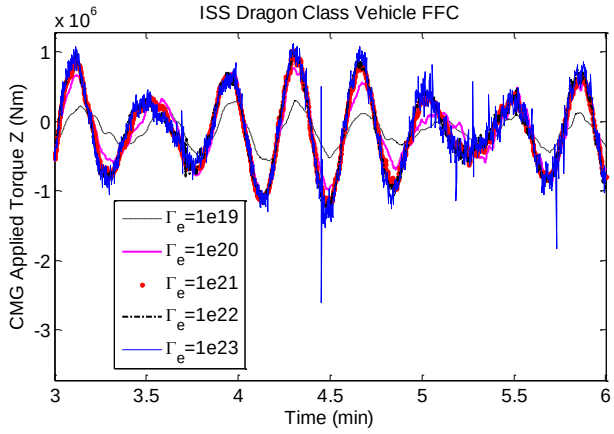

Figure 14 ISS CMG Applied Torque Z for Various SAC Γ_e Gains.

Baseline Results

Both PD and SAC controller are capable to regulate ISS body attitude and attitude rate within 3 minutes after the full rigidization of the LEE mechanism. When compared with each other, the SAC controller performs by order of magnitude better than the PD controller in both signal overshoot and overall settling time in attitude convergence. Figure 15 to Figure 17 shows the ISS attitude 3 minutes after the initiation of the capture process. The results show the SAC controller reduces the ISS attitude as soon as the LEE finishes the rigidization where the PD controller takes roughly twice as long to bring the attitude to the same SAC steady state levels. It should be noted both PD and SAC controllers briefly demanded torque beyond the allowable ISS CMG torque limit, and thus were limited at the maximum torque level. Despite torque limiting, both PD and SAC controllers stayed within the maximum momentum capacity of the CMG.

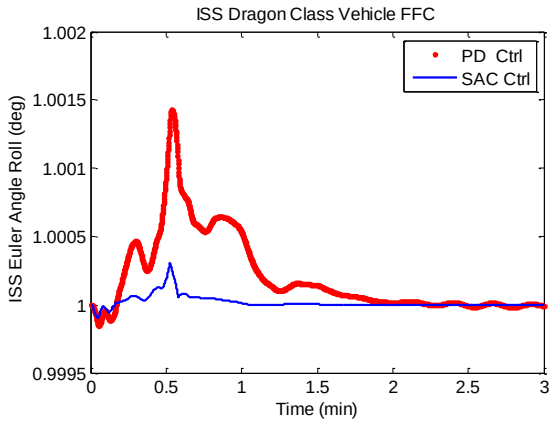

Figure 15 ISS Roll Angle PD to SAC Comparison.

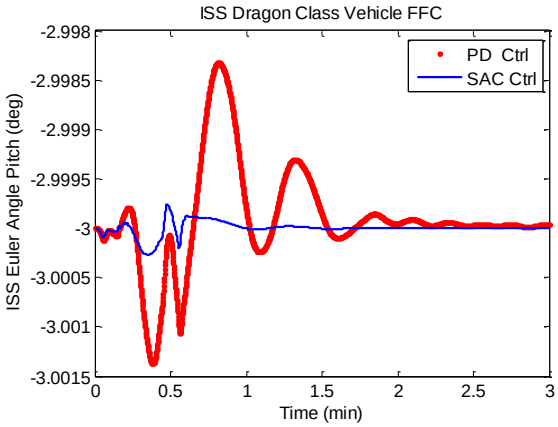

Figure 16 ISS Roll Angle PD to SAC Comparison.

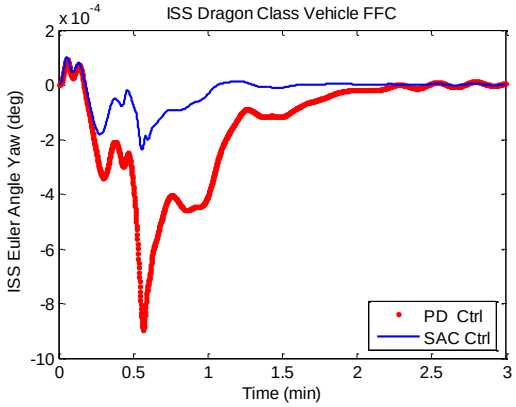

Figure 17 ISS Roll Angle PD to SAC Comparison.

Controller Robustness

To further demonstrate the improved performance of SAC over the PD controller, various mass and capture misalignment scenarios beyond the tuning baseline were simulated. Figure 18, Figure 19, and Figure 20 shows the Roll, Pitch and Yaw of each variation subtracting the baseline for PD control while Figure 21, Figure 22, and Figure 23 are the counterparts for SAC. In each comparison, four additional case scenarios were simulated, mass and inertia at 50%, 150%, and 200% of the baseline. Additionally, for the 200% scenario, the capture orientation misalignments were increased to 10 degrees in roll and 15 degrees in wobble** which represents the highest possible misalignment of the capture interface capacity. It can be shown for all cases with the exception of yaw 200% high-misalignment case, the SAC degradation due to worsened mass and capture conditions are roughly four times less than the PD control degradation thus making it more robust than the PD controller to operational uncertainties.

VII. CONCLUSION

In summary, this study examined SAC performance in a complex simulation environment thereby building confidence in the adaptive approach. This study highlighted the improved performance and robustness to parametric and dynamic uncertainties achieved with SAC when compared to the PD control.

ACKNOWLEDGEMENTS

The author wishes to acknowledge Kerman Buhariwala and Neil Roger from MDA Space Missions for their mentorship in programming the SPOTS simulator. The author also wishes to acknowledge the Canadian Space Agency for the tremendous support and investment into the MDA SPOTS simulation facility.

**Wobble is the Root Sum Square (RSS) of pitch and yaw misalignments in the EEOCS frame.

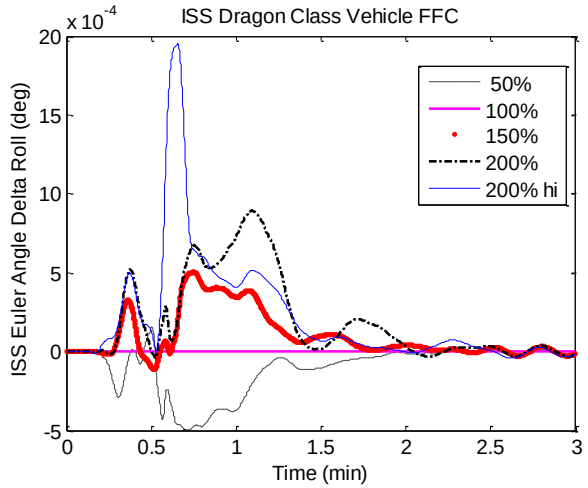

Figure 18 ISS Delta Roll to Baseline Mass–PD Control.

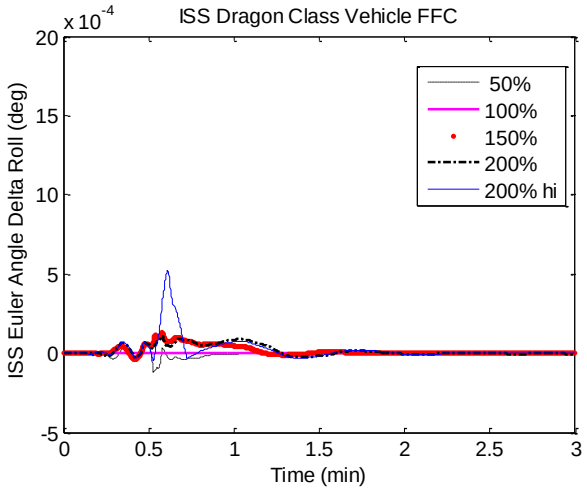

Figure 21 ISS Delta Roll to Baseline Mass–SAC.

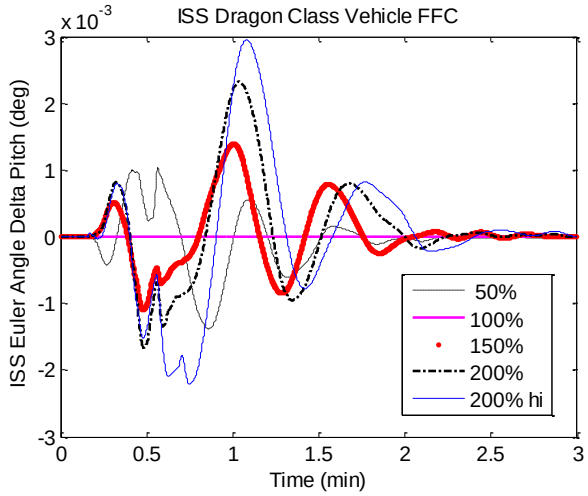

Figure 19 ISS Delta Pitch to Baseline Mass–PD Control

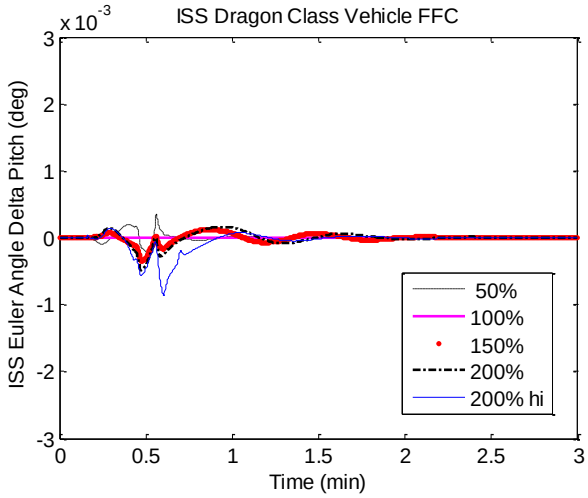

Figure 22 ISS Delta Pitch to Baseline Mass–SAC.

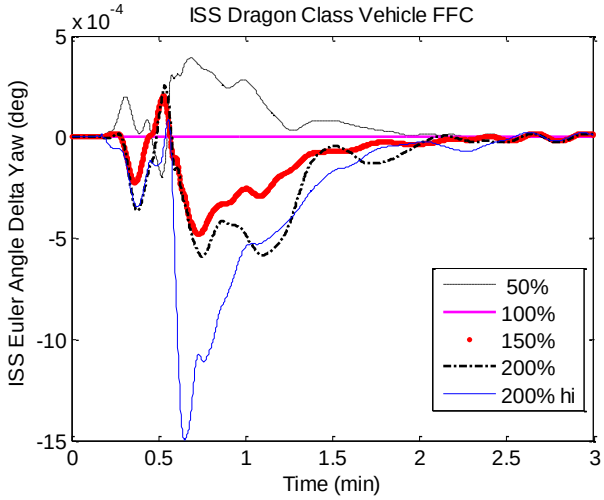

Figure 20 ISS Delta Yaw to Baseline Mass–PD Control.

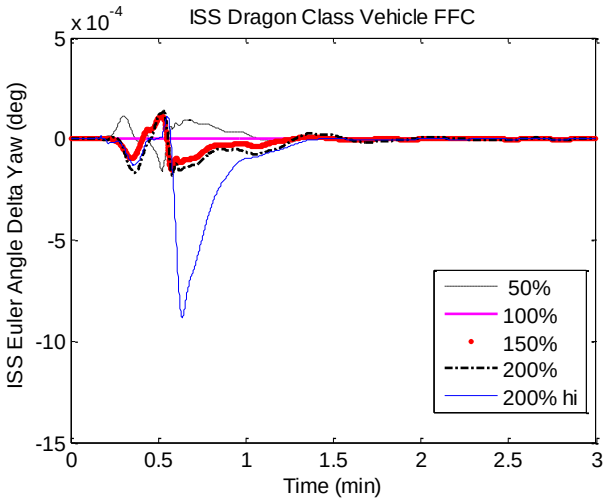

Figure 23 ISS Delta Yaw to Baseline Mass–SAC.

REFERENCES

[1] Kasai, T., Oda, M., and Suzuki, T., "Results of the ETS-7 Mission Rendezvous Docking and Space Robotics Experiments," *5th International Symposium on Artificial Intelligence, Robotics and Automation in Space*, 1-3 Jun, 1999 (ESA SP440)

[2] Ogilvie, A., Allport, J., Hannah, M., and Lymer, J., "Autonomous Satellite Servicing Using the Orbital Express Demonstration Manipulator System,"*9th International Symposium on Artificial Intelligence, Robotics and Automation in Space*, 2008

[3] Whipple, A., "A Comparison of Human and Robotic Servicing of the Hubble Space Telescope," NASA Goddard Space Flight Centre Astrophysics Projects Division Office, October 14, 2009

[4] Aziz, S., "Considerations for Next Generation Space Manipulators," *IEEE International Conference on Robotics and Automation*, 2011.

[5] Flores-Abad, A., Ma, O., Pham, K., Ulrich, S, "A Review of Space Robotics Technologies for On-orbit Servicing," *Progress in Aerospace Sciences*,68, 2014, pp.1-26.

[6] Smith, C. and Seagram, J., "Free-Flyer Capture - New Robotic Challenges from the International Space Station," *Journal of the British Interplanetary Society*, Vol. 60, 2007, pp. 333-346.

[7] Gurrisi, C.,Seidel, R.,Dickerson, S.,Didziulis, S.,Frantz, P., and Ferguson, K., "Space Station Control Moment Gyroscope Lessons Learned," *40th Aerospace Mechanisms Symposium*, NASA Kennedy Space Centre, 12-14 May, 2010.

[8] Tsuda, Y., and Nakasuka, S., "New Attitude Motion Following Control Algorithm for Capturing a Tumbling Object in Space," *Acta Astronautica*, 2003, Vol. 53, No. 11, pp. 847-861

[9] Bedrossian, N., Bhatt, S., Kang, W., Ross, I.M., "Zero-Propellant Manoeuvre Guidance," *IEEE Control Systems Magazine*, October 2009, pp. 53-73.

[10] Bedrossian, N., Bhatt, S., Lammers, M., Nguyen, L., Zhang, Y., "First Ever Flight Demonstration of Zero Propellant Maneuver™ Attitude Control Concept," *AIAA Guidance, Navigation and Control Conference and Exhibit*, Hilton Head, SC, 20-23 Aug, 2007, AIAA 2007-6734.

[11] Bedrossian, N., Jang, J-W., Alaniz A., Johnson, M., Sebelius, K., Mesfin, Y., "International Space Station US GN&C Attitude Hold Controller Design for Orbiter Repair Manoeuvre," *AIAA Guidance, Navigation, and Control Conference and Exhibit*, San-Francisco, CA, 15-18 Aug, 2005, AIAA-2005-5853.

[12] Bedrossian, N., McCants, E., "Space Station Attitude Control During Payload Operations,", *AAS/AIAA Astrodynamics Conference*, Girdwood, Alaska, AAS 99-372, 16-19 Aug, 1999.

[13] Bedrossian, N., Bhatt, S., Alaniz, A., McCants, E., Nguyen, L., Chamitoff, G., "ISS Contingency Attitude Control Recovery Method for Loss of Automatic Thruster Control,", *31st Annual AAS Guidance and Control Conference*, Breckenridge, CO, 1-6 Feb 1-6, 2008.

[14] Ulrich, S., Hayhust, D. L., Saenz-Otero, A., Miller, D. W., and Barkana, I., "Simple Adaptive Control for Spacecraft Proximity Operations," *AIAA Guidance, Navigation, and Control Conference*, National Harbor, MD, 13-17 Jan, 2014, AIAA Paper 2014-1288.

[15] Shi, J.F., Ulrich, S., Allen, A, "Spacecraft Adaptive Attitude Control with Application to Space Station Free-flyer Robotic Capture," *AIAA Guidance, Navigation, and Control Conference*, Kissimmee, FL, accepted.

[16] Hughes, P., *Spacecraft Attitude Dynamics*, Dover, 2004.

[17] Ma, O., Buhariwala, K., Roger, N., Maclean, J., and Carr, R., "MDSF a Generic Development and Simulation Facility for Flexible Complex Robotic Systems," *Robotica*, 1997, Vol. 15, pp. 49-62.

[18] Ma, O., "CDT-A General Contact Dynamics Toolkit," *International Symposium on Robotics*, Montreal, Canada, May 2000, pp. 468-473.

[19] Wang, J., Mukherji, R., Ficocelli, M., and Ogilvie, A., "Modeling and Simulation of Robotic System for Servicing Hubble Space Telescope," *IEEE/RSJ International Conference on Intelligent Robots and Systems*, Beijing, China, 9-15 Oct, 2006.

[20] Ueda, S., Kasai, T., and Uematsu, H., "HTV Rendezvous Technique and GN&C Design Evaluation Based on 1st Flight On-Orbit Operation Result," *AIAA/AAS Astrodynamics Specialist Conference*, Toronto, Canada, 2-5 Aug, 2010, AIAA 2010-7664.

[21] SSP 30219, "International Space Station Program - Space Station Reference Coordinate System," Revision H, NASA JSC, Houston, Texas, June 1, 2005.

[22] Couluris, J., and Garvey, T., "SpaceX Mission Operations", *AIAA Space Ops 2010 Conference*, Huntsvill, Alabama, 25-30 Apr, 2010, AIAA 2010-1937.

[23] ESA-HSO-COU-028-Rev 2.0-ISS Space X Dragon Fact Sheet, *http://wsn.spaceflight.esa.int/docs/Factsheets/28%20SpaceXDragon%20LR.pdf*

[24] NASA Fact Sheet "An Orbiting Laboratory", NASA JSC, 2011, *http://www.nasa.gov/sites/default/files/files/562644main_FS-2011-ISS_Orbiting_Lab.pdf*

[25] Kim, JW., Crassidis, JL., Vadali, SR., and Dershowitz, AL., "International Space Station Leak Localization using Attitude Response Data", *AIAA Journal of Guidance, Control, and Dynamics*, Vol. 29, No.5, Sept-Oct 2006, pp. 1041-1050.